Chapter-3

SOLAR PLASMA CHARACTERIZATION WITH INHOMOGENEITY SCALE ANALYSIS IN TURBOMAGNETIC GES-FABRIC

Abstract: *This chapter presents a continued study founded on the idealistic GES-model based solar plasma system. It is a recent GES extension by integrating realistic non-thermal electronic thermo-statistics, magneto-activity, and plasma fluid turbulence. Numerical analysis of the systematically derived governing equations for the SIP and the SWP media is performed to obtain the inhomogeneity scale length profiles of the various key solar plasma properties with an aim to explore their spatial non-uniformity features*[†].

3.1 INTRODUCTION

The Sun, its surrounding atmosphere and ensuing plasma flow in the interplanetary medium, called the solar wind are highly inhomogeneous in nature. The large-scale inhomogeneity is caused at the cost of diversified force gradients. One of such heterogeneity is noticed in the non-extensivity and non-thermality of the solar plasma system in the realistic thermo-statistical perspective [1]. Such non-thermal features cast various challenges to reveal diversified complex plasma dynamical processes in the Sun and its atmosphere, yet to be well explored against the present observational scenarios. One of such less-explored area is the effects of non-thermally distributed electron population in the solar or stellar plasma flow dynamical evolutionary processes [1-3].

In this presented study, the typical properties of the polytropic turbulent magneto-active gravito-electrostatic sheath (GES)-model based solar properties, as previously seen in **Chapter-2**, are illustratively explored by particularly looking into their inhomogeneity scale length behaviours, over which they change. For a quantity "*X*" the spatial inhomogeneity scale length in a spherically symmetric system is mathematically expressed as $X(\partial X/\partial r)^{-1}$, where r is the distance from the origin [4]. So, for a high value of the scale length, the value of *X* per unit gradient must be high and vice-versa. As the spatial gradient decreases, the inhomogeneity scale length increases and vice-versa

[†]Sarma, P. and Karmakar, P. K. Solar plasma characterization in Kappa (κ)-modified polytropic turbomagnetic GES-model perspective. *Monthly Notices of the Royal Astronomical Society*, 519(2):2879-2916, 2023.

for a smooth variation of the quantity "*X*". Here, the analysis reveals the spatial gradient variation, and hence the degree of radial uniformity of the various equilibrium solar plasma properties as elaborately explored below.

The graphical interpretation of inhomogeneity scale length is depicted in figure 3.1. It is observed that for a particular value of *X* (= *c*), the inhomogeneity scale length at the point A (with higher slope) on the curve (= RS) is smaller than that (= RT) at the point B (with lower slope). The region around point A has low spatial homogeneity, i.e., possible inhomogeneity in small scale lengths. On the other hand, the region around point B has high spatial homogeneity, i.e., possible inhomogeneity in high scale lengths.

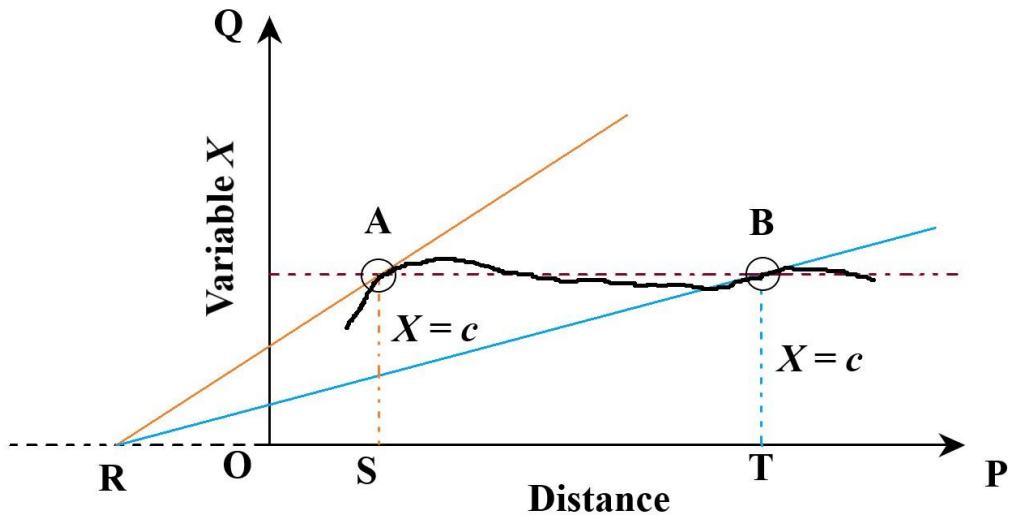

***Figure 3.1**: Graphical explanation of inhomogeneity scale length.*

3.2 SOLAR PLASMA MODEL FORMULATION

The solar plasma medium is assumed to be composed of non-thermal κ-distributed, lighter non-gravitating electrons and heavier, inertial gravitating ions throughout the entire considered spherically symmetric system. Thus, the model involves only the radially dependent variables. The magneto-active plasma medium is turbulent in nature modelled here via the Larson-logatropism [5]. The mechanisms of the plasma sheath formation, eased basically due to the tuned gravito-thermal electron-ion coupling, are well mentioned in the widely available literature [6, 7] and in the previous chapters as well. All the model governing equations are described below in their time-stationary normalized form for exploring the equilibrium properties of the solar plasma system.

3.2.1 NORMALIZED SOLAR INTERIOR PLASMA (SIP) GOVERNING EQUATIONS

The set of the key governing equations narrating the characteristics of the bounded SIP scale consists of the non-thermal electronic κ-distribution law, ion continuity equation, ion momentum equation, equation of state, electrostatic Poisson equation, gravitational Poisson equation, and the current density evolution equation in a closed form. All the symbols, their significances and the astronomically relevant normalization scheme of the governing equations are well explained in Tables 2.1 and 2.2 respectively. Accordingly, the normalized κ-distributed electron population is expressed as

$$N_e = \left[1-\left(\frac{2}{2\kappa-3}\right)\Phi\right]^{-\kappa+1/2}. \tag{3.1}$$

The ion continuity equation in normalized form is given as

$$M\left(\partial_\xi N\right)+N\left(\partial_\xi M\right)+\left(\frac{2}{\xi}\right)M\,N=0. \tag{3.2}$$

The normalized form of the ion momentum equation is written as

$$\begin{aligned} M\left(\partial_\xi M\right) = &-T_e^*\left(\partial_\xi\Phi\right)-\left(\frac{\alpha\lambda_J\Gamma n_0^{\Gamma-1}}{m_i c_s^2}\right)N^{\Gamma-2}\left(\frac{2\kappa-1}{2\kappa-3}\right)\left[1-\left(\frac{2}{2\kappa-3}\right)\Phi\right]^{-\kappa-1/2}\frac{1}{\lambda_J}\left[\partial_\xi\Phi+T_e^*\Phi\,\partial_\xi\left(\frac{1}{T_e^*}\right)\right] \\ &-\frac{1}{N}\left[T_i^*\left(\partial_\xi N\right)+N\left(\partial_\xi T_i^*\right)\right]\left[1+\ln(N)\right]-T_i^*\frac{1}{N}\left(\partial_\xi N\right)-\partial_\xi\Psi+\left(\frac{\eta}{m_i n_0 c_s\lambda_J}\right)\frac{1}{\xi^2}\frac{1}{N}\left[\partial_\xi\left(\xi^2\,\partial_\xi M\right)\right] \end{aligned}. \tag{3.3}$$

The equation of state in the normalized form is expressed as

$$P_T^* = \left(\frac{\alpha\, n_0^\Gamma}{P_0}\right)\left[1-\left(\frac{2}{2\kappa-3}\right)\Phi\right]^{(-\kappa+1/2)\Gamma}+P_{Th}^*\left[1+ln\left(N_i\right)\right]+\beta_0\left(B^*\right)^2. \tag{3.4}$$

The normalized electrostatic Poisson equation is cast as

$$N_e-N_i=\left(\frac{\lambda_{De}}{\lambda_J}\right)^2\left[\partial_\xi^2\Phi+\left(\frac{2}{\xi}\right)\partial_\xi\Phi\right]. \tag{3.5}$$

The normalized gravitational Poisson equation is written as

$$\partial_\xi^2\Psi+\left(\frac{2}{\xi}\right)\partial_\xi\Psi=N. \tag{3.6}$$

The current density evolution equation in the SIP in normalized form is expressed as

$$J_{SIP}=N\left[-\sqrt{2\,\xi\left(\partial_\xi\Psi\right)}-\sqrt{\left\{2\left(\frac{T_e}{T_i}\right)\xi\left(\partial_\xi\Phi\right)\right\}}+\sqrt{\left\{2\left(\frac{m_i}{m_e}\right)\left(\frac{T_e}{T_i}\right)\xi\left(\partial_\xi\Phi\right)\right\}}\right]. \tag{3.7}$$

The above equations are coupled to obtain a basic set of static first order differential equations. The fourth-order Runge-Kutta (RK-IV) method is applied with initial input values as depicted in Table 2.3 for obtaining the various plots signifying the inhomogeneity scale length behaviours of the various relevant solar properties [7].

3.2.2 NORMALIZED SOLAR WIND PLASMA (SWP) GOVERNING EQUATIONS

In the SWP system, the Sun (SIP) acts as a point source of Newtonian gravity of mass M_{Θ}. Consequently, the dynamics of the SWP fluid is governed by the same equations as that of the SIP medium, except the solar self-gravity gets replaced by the corresponding inverse-square solar gravity. As a result, the gravitational Poisson equation becomes redundant [6]. Accordingly, the basic governing equations in the normalized form, in the same order as in **Section 3.2.1**, following the same astrophysical normalization scheme, can be written as follows.

$$N_e = \left[1-\left(\frac{2}{2\kappa-3}\right)\Phi\right]^{-\kappa+1/2}, \tag{3.8}$$

$$M\left(\partial_\xi N\right)+N\left(\partial_\xi M\right)+\left(\frac{2}{\xi}\right)M\,N=0, \tag{3.9}$$

$$M\left(\partial_\xi M\right)=-T_e^*\left(\partial_\xi\Phi\right)-\left(\frac{\alpha\lambda_J\Gamma n_0^{\Gamma-1}}{m_i c_s^2}\right)N^{\Gamma-2}\left(\frac{2\kappa-1}{2\kappa-3}\right)\left[1-\left(\frac{2}{2\kappa-3}\right)\Phi\right]^{-\kappa-1/2}\frac{1}{\lambda_J}\left[\partial_\xi\Phi+T_e^*\Phi\,\partial_\xi\left(\frac{1}{T_e^*}\right)\right], \tag{3.10}$$
$$-\frac{1}{N}\left[T_i^*\left(\partial_\xi N\right)+N\left(\partial_\xi T_i^*\right)\right]\left[1+\ln\left(N\right)\right]-T_i^*\frac{1}{N}\left(\partial_\xi N\right)-\left(\frac{1}{c_s^2\lambda_J}\right)\frac{GM_\Theta}{\xi^2}+\left(\frac{\eta}{m_i n_0 c_s\lambda_J}\right)\frac{1}{\xi^2}\frac{1}{N}\left[\partial_\xi\left(\xi^2\,\partial_\xi M\right)\right]$$

$$P_T^*=\left(\frac{\alpha\, n_0^{\Gamma}}{P_0}\right)\left[1-\left(\frac{2}{2\kappa-3}\right)\Phi\right]^{(-\kappa+1/2)\Gamma}+P_{Th}^*\left[1+ln\left(N_i\right)\right]+\beta_0\left(B^*\right)^2, \tag{3.11}$$

$$N_e-N_i=\left(\frac{\lambda_{De}}{\lambda_J}\right)^2\left[\partial_\xi^2\Phi+\left(\frac{2}{\xi}\right)\partial_\xi\Phi\right], \tag{3.12}$$

$$J_{SWP}=N\left[-\sqrt{2\xi\left(\frac{1}{c_s^2\lambda_J}\right)\frac{GM_\Theta}{\xi^2}}-\sqrt{\left\{2\left(\frac{T_e}{T_i}\right)\xi\left(\partial_\xi\Phi\right)\right\}}+\sqrt{\left\{2\left(\frac{m_i}{m_e}\right)\left(\frac{T_e}{T_i}\right)\xi\left(\partial_\xi\Phi\right)\right\}}\right]. \tag{3.13}$$

The above equations are coupled to get a set of first-order differential equations governing the steady-state picture of the SWP. Then the RK-IV method is applied for numerical analysis with the initial inputs as in Table 2.3 [7].

3.3 RESULTS AND DISCUSSIONS

In order to explore the inhomogeneity scale length behaviours of the various relevant quantities, at first, the formation of the solar surface boundary (SSB) is observed with its response on κ-variation. It is well depicted in figure 3.2. Here, the spatial grid size used is 0.10. It is clear that the SSB drifts inward with an increase in electron non-thermal behaviour (i.e., decreasing κ-value). The physics behind is well explicated in **Chapter-2** and in available literature [7]. After getting the distinct bi-scaled solar plasma system, the various inhomogeneity scale length behaviours for the SIP and the SWP are studied in two separate subsections as follows.

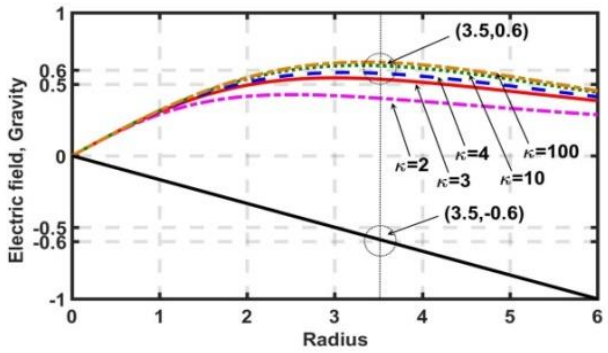

Figure 3.2: *Profile of the normalized (a) κ-sensitive gravitational field strength (gravity) and (b) κ-insensitive electric field strength with variation in the Jeans-normalized heliocentric radial distance for different κ-values as shown.*

3.3.1 INHOMOGENEITY SCALE LENGTH BEHAVIOURS OF THE SIP-PROPERTIES

As depicted in figure 3.3, we portray the spatial profile of the normalized SIP self-gravitational inhomogeneity scale length (= $g_s(\partial g_s/\partial\xi)^{-1}$) for different κ-values; where g_s is the normalized self-gravity strength. It is noticed that, for κ = 3, the scale length reaches a very high positive value near ξ = 3. So, the self-gravity becomes highly homogeneous in that near-SSB zone (as the gradient becomes reduced). As we move towards the electron-thermality regime ($\kappa \to \infty$), this scale length is negative in the near-SSB zone, meaning high material inhomogeneity in the near-SSB region. It may be attributable to the high transferability of electron thermo-mechanical energy to the inertial ions, with an increase in the κ-value.

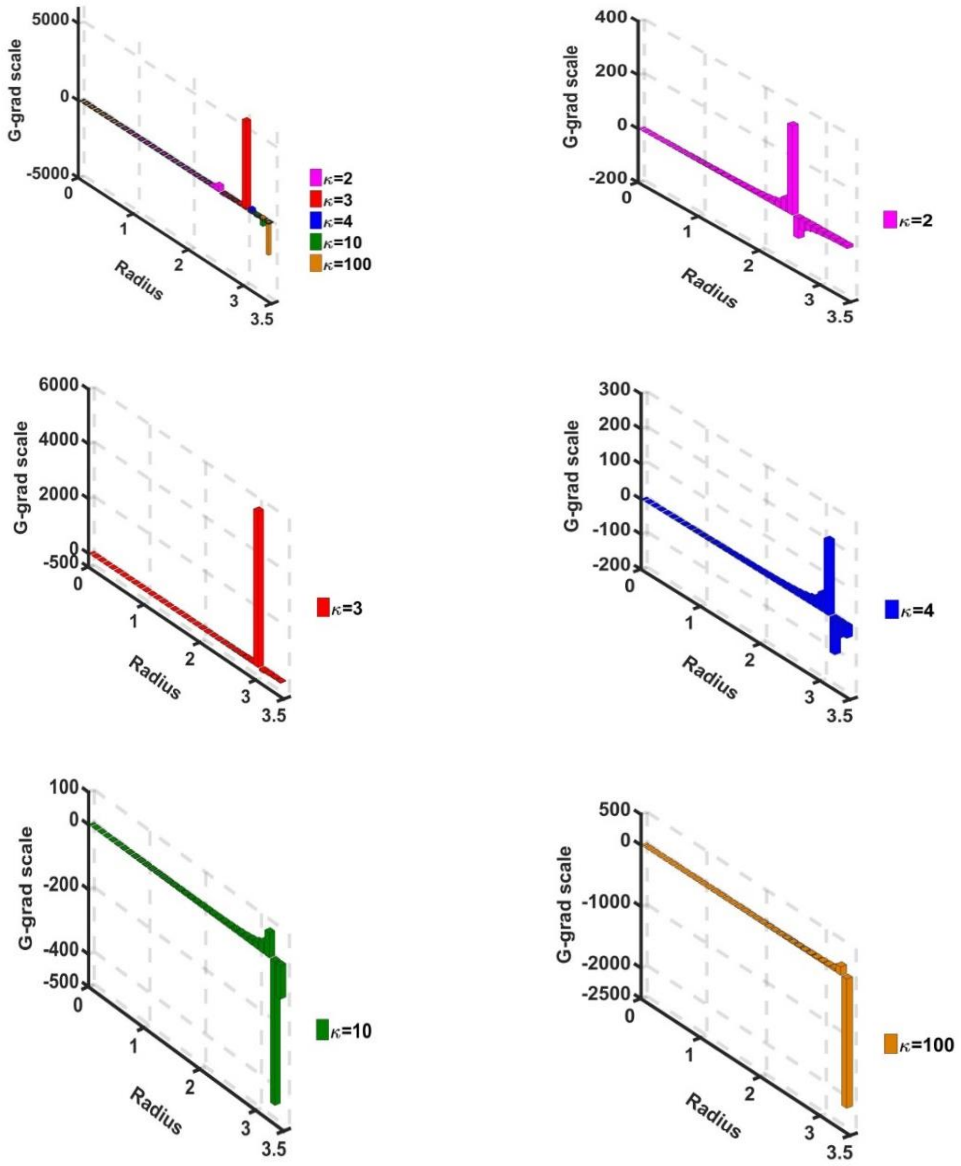

Figure 3.3: *Variation of the normalized self-gravitational inhomogeneity (*G*-grad) scale length with the Jeans-normalized heliocentric radial distance for fixed T_e/T_i=1 and different κ-values as shown.*

As shown in figure 3.4, we represent the SIP electric potential inhomogeneity scale length (= $\Phi(\partial\Phi/\partial\xi)^{-1}$) with the Jeans-normalized heliocentric radial distance for different κ-values. It is found to be independent of the electron non-thermality as the potential itself and it maintains a steady growth throughout the entire SIP.

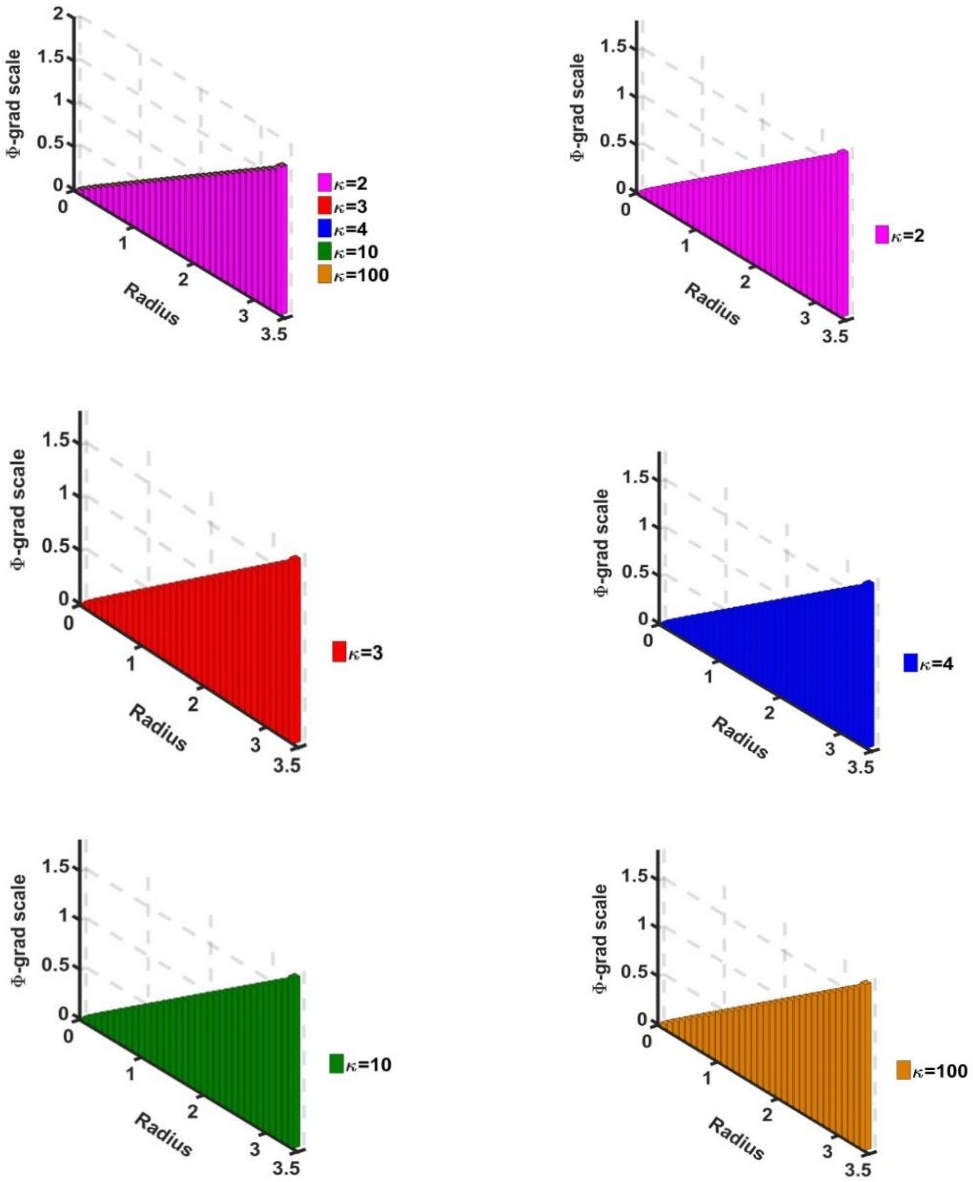

Figure 3.4: *Variation of the normalized SIP electric potential inhomogeneity (Φ-grad) scale length with the Jeans-normalized heliocentric radial distance for fixed T_e/T_i =1 and different κ-values as shown.*

In figure 3.5, we plot the SIP electric field inhomogeneity scale length (= $E(\partial E/\partial \xi)^{-1}$) with the Jeans-normalized heliocentric radial distance for different κ-values. It is found to be independent of the electron non-thermality, exhibiting a steady growth throughout the entire SIP medium.

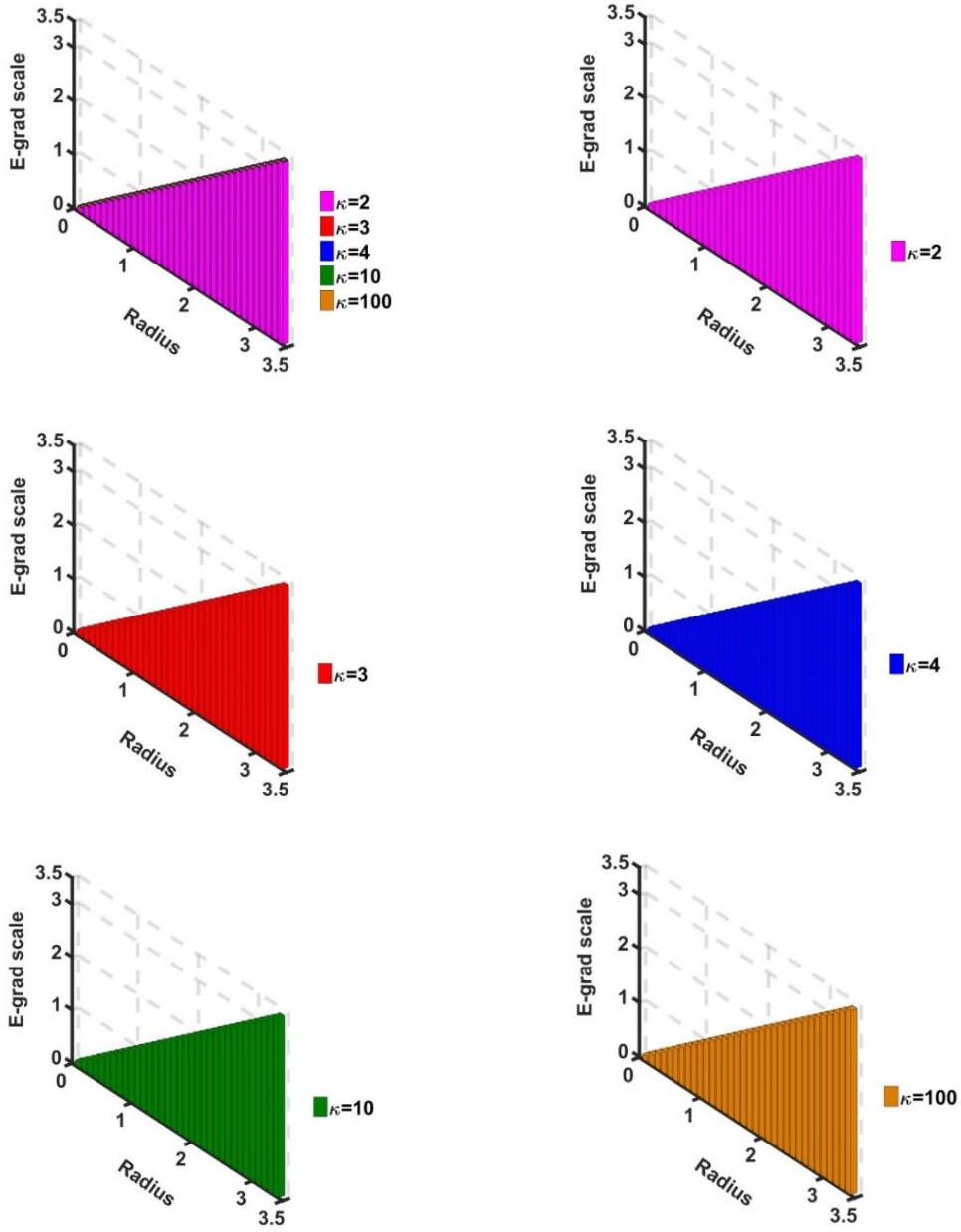

Figure 3.5: *Variation of the normalized SIP electric field inhomogeneity (E-grad) scale length with the Jeans-normalized heliocentric radial distance for fixed $T_e/T_i=1$ and different κ-values as shown.*

As in figure 3.6, we plot the SIP Mach number inhomogeneity scale length (= $M(\partial M/\partial\xi)^{-1}$) with the Jeans-normalized heliocentric radial distance for different κ-values. A slight inhomogeneity difference is noticed for a very high non-thermality (κ = 2) only; though the response is same towards electron thermality regime.

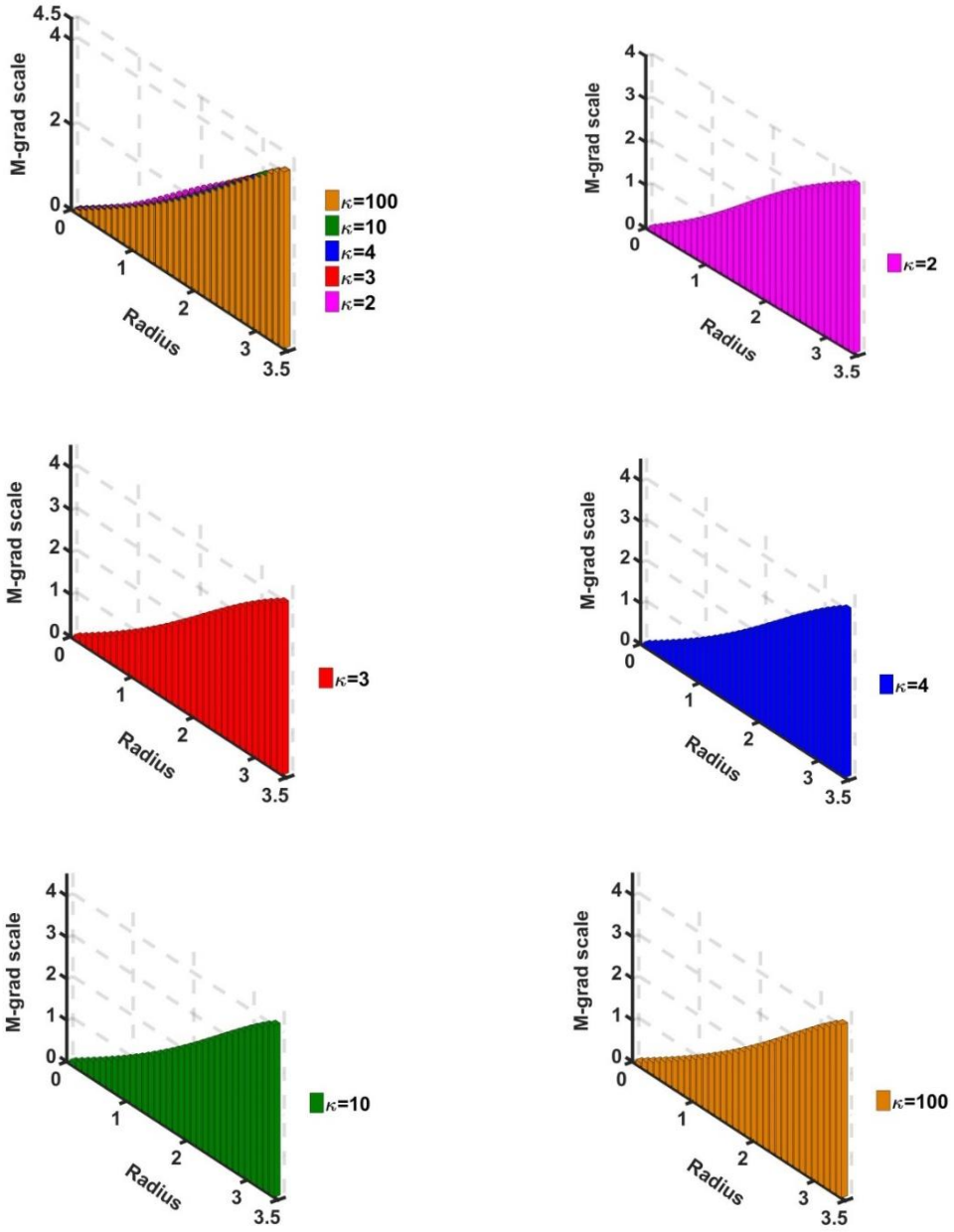

Figure 3.6: *Variation of the normalized SIP Mach number inhomogeneity (M-grad) scale length with the Jeans-normalized heliocentric radial distance for fixed $T_e/T_i=1$ and different κ-values as shown.*

In figure 3.7, we represent the SIP electric current density inhomogeneity scale length (= $J(\partial J/\partial\xi)^{-1}$) with the Jeans-normalized heliocentric radial distance for different κ-values. A directional flip in this scale length is noticed inside the SIP volume. This direction flipping region moves away from the heliocenter with an increase in κ. This behaviour may be attributable to the increase of the SIP volume with the increasing κ-value, as explored previously in case of figure 3.2.

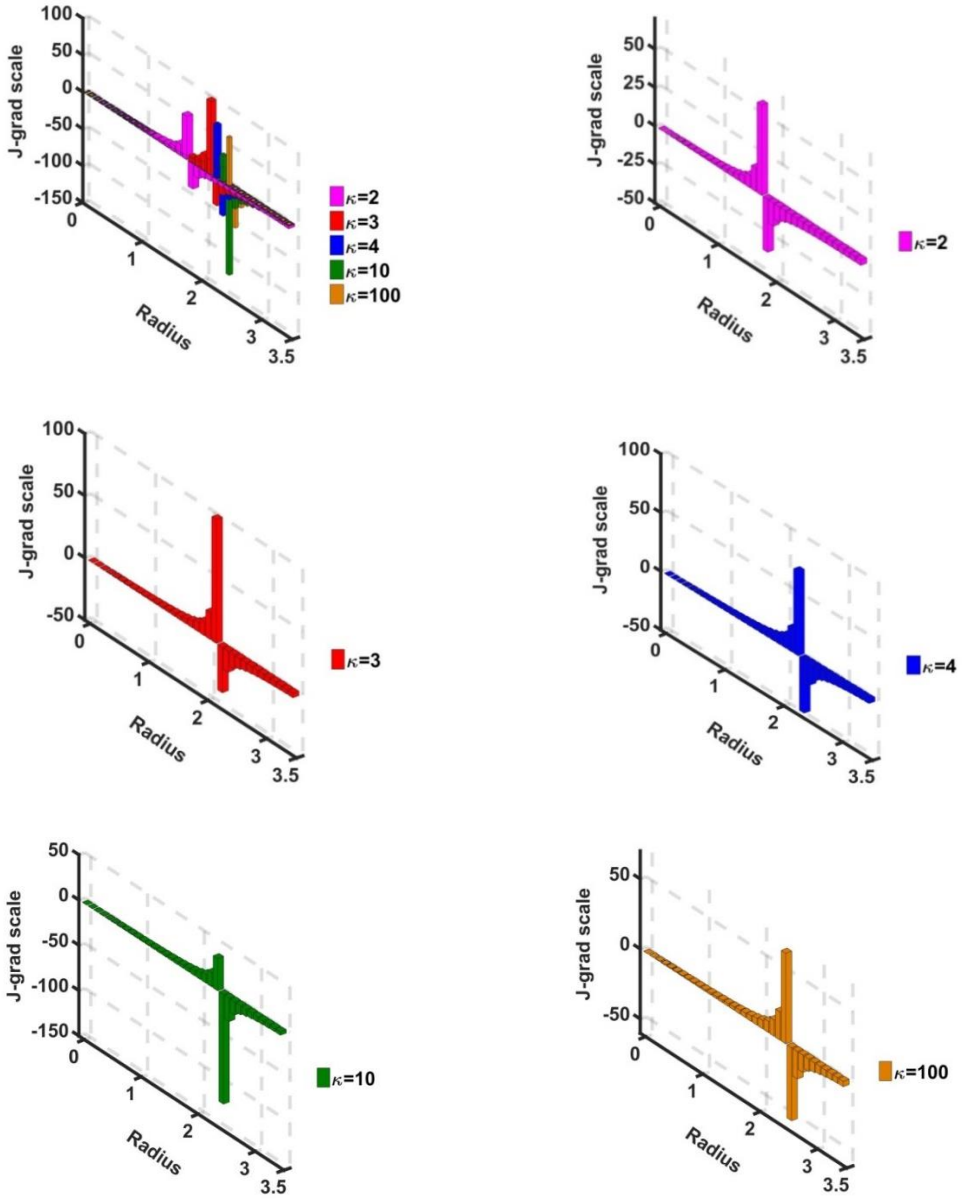

Figure 3.7: *Variation of the normalized SIP electric current density inhomogeneity (J-grad) scale length with the Jeans-normalized heliocentric radial distance for fixed $T_e/T_i=1$ and different κ-values as shown.*

In figure 3.8, we present the similar profile as in figure 3.7, but for different T_e/T_i-values with a particular κ-value. It is found that the magnitude of this scale length slightly increases with increase in this ratio at the current density direction flipping point. This may be due to the high electron temperature facilitating effective energy transport to the cold ions causing homogeneous current density in that particular region of the SIP.

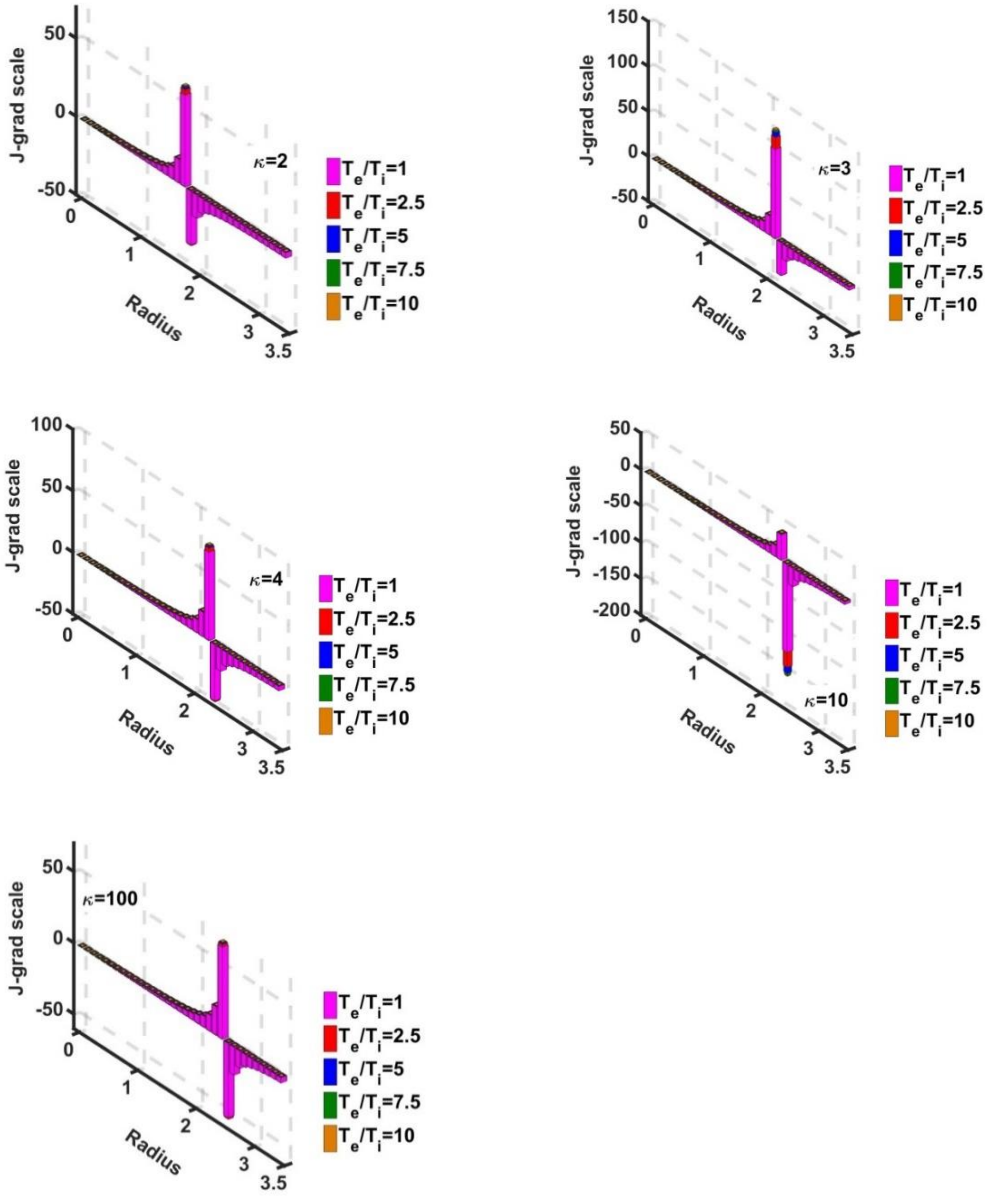

Figure 3.8: *Variation of the normalized SIP electric current density inhomogeneity (J-grad) scale length with the Jeans-normalized heliocentric radial distance for fixed κ and different T_e/T_i–values as shown.*

3.3.2 INHOMOGENEITY SCALE LENGTH BEHAVIOURS OF THE SWP-PROPERTIES

As shown in figure 3.9, we present the spatial profile of the normalized SWP gravitational inhomogeneity scale length (= $g(\partial g/\partial\xi)^{-1}$) for different κ-values, where g is the normalized gravity strength. Here, the spatial grid size used is 20. It is noticed that the scale length reaches a high positive value in the near-SIP zone. So, the gravity becomes highly homogeneous in the near-SIP zone. As one moves outward from the SIP,

this scale length becomes negative with increase in its magnitude. So, the material inhomogeneity is very high and the density goes on decreasing with the heliocentric radial distance away in the entire SWP region. For κ = 3 onwards, the scale length is slightly more positive. So, gravity is slightly more homogeneous in the SWP for these electron non-thermality extents.

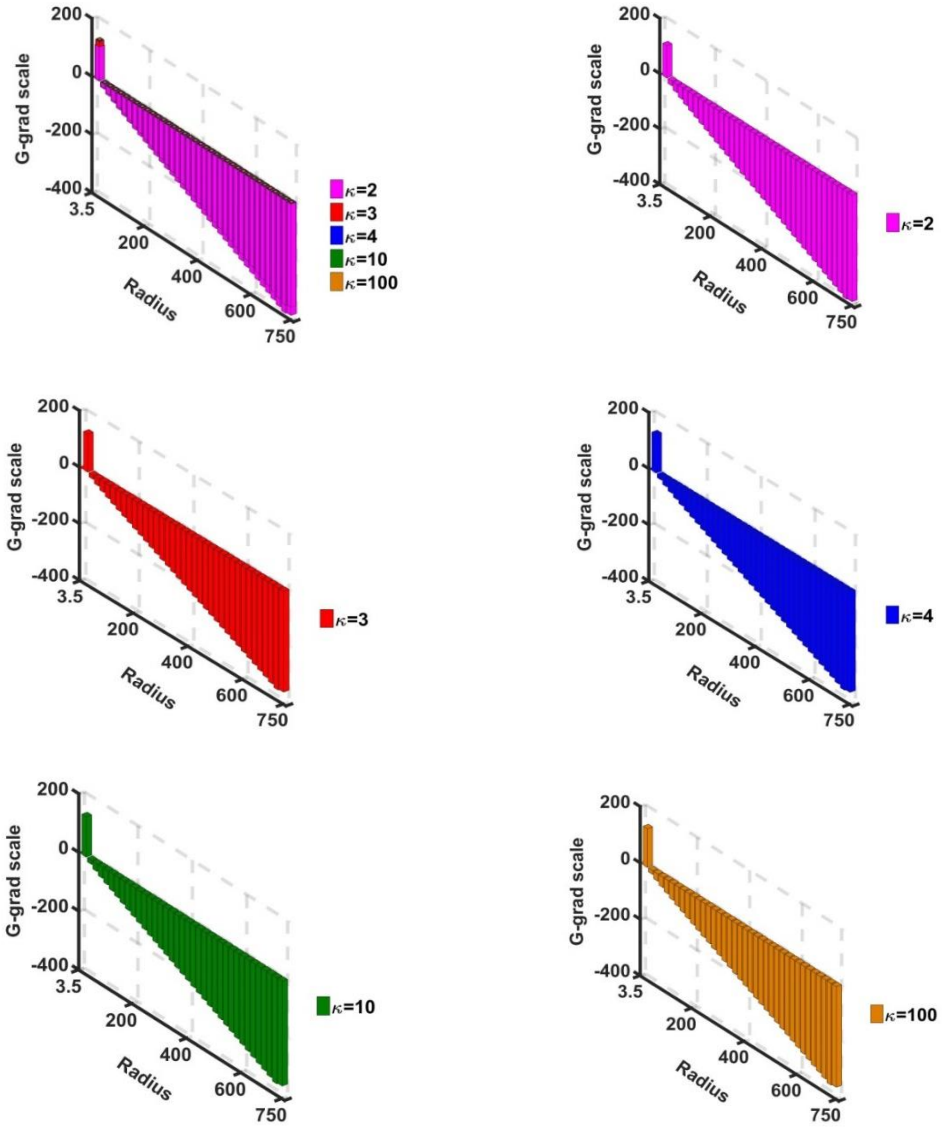

Figure 3.9: *Variation of the normalized SWP gravitational inhomogeneity (G-grad) scale length with the Jeans-normalized heliocentric radial distance for fixed T_e/T_i=1 and different κ-values as shown.*

In figure 3.10, we depict the SWP electric potential inhomogeneity scale length (= $\Phi(\partial\Phi/\partial\xi)^{-1}$) with the Jeans-normalized heliocentric radial distance for different κ-

values. It is found to be independent of the electron non-thermality and maintains a steady growth throughout the entire SWP medium.

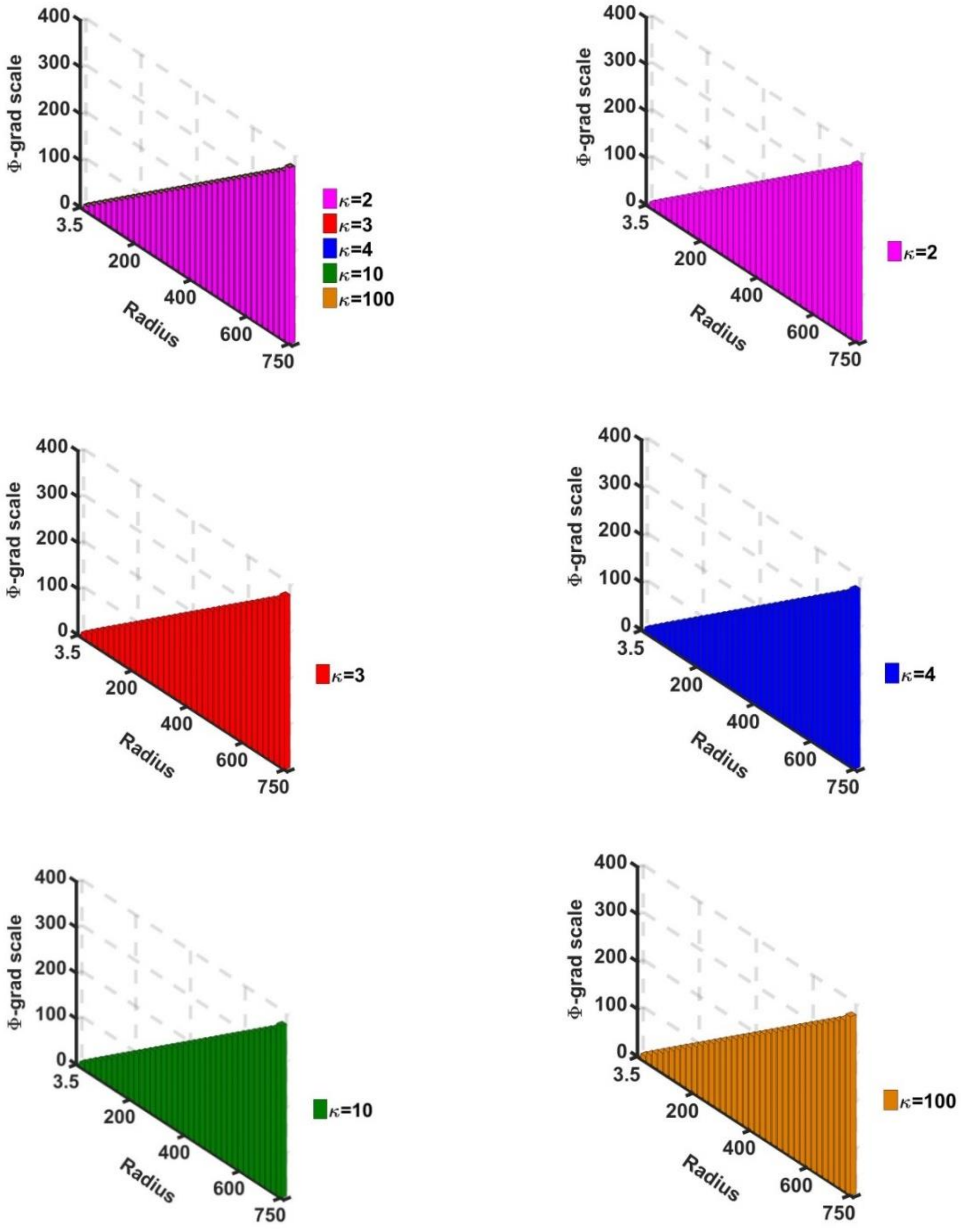

Figure 3.10: *Variation of the normalized SWP electric potential inhomogeneity (Φ-grad) scale length with the Jeans-normalized heliocentric radial distance for fixed $T_e/T_i=1$ and different κ-values as shown.*

As in figure 3.11, we plot the SWP electric field inhomogeneity scale length (= $E(\partial E/\partial\xi)^{-1}$) with the Jeans-normalized heliocentric radial distance for different κ-values. It is found to be independent of the electron non-thermality and maintains a steady

growth throughout the entire SWP. So, the field becomes more and more homogeneous as the observer moves towards the far-SIP zone.

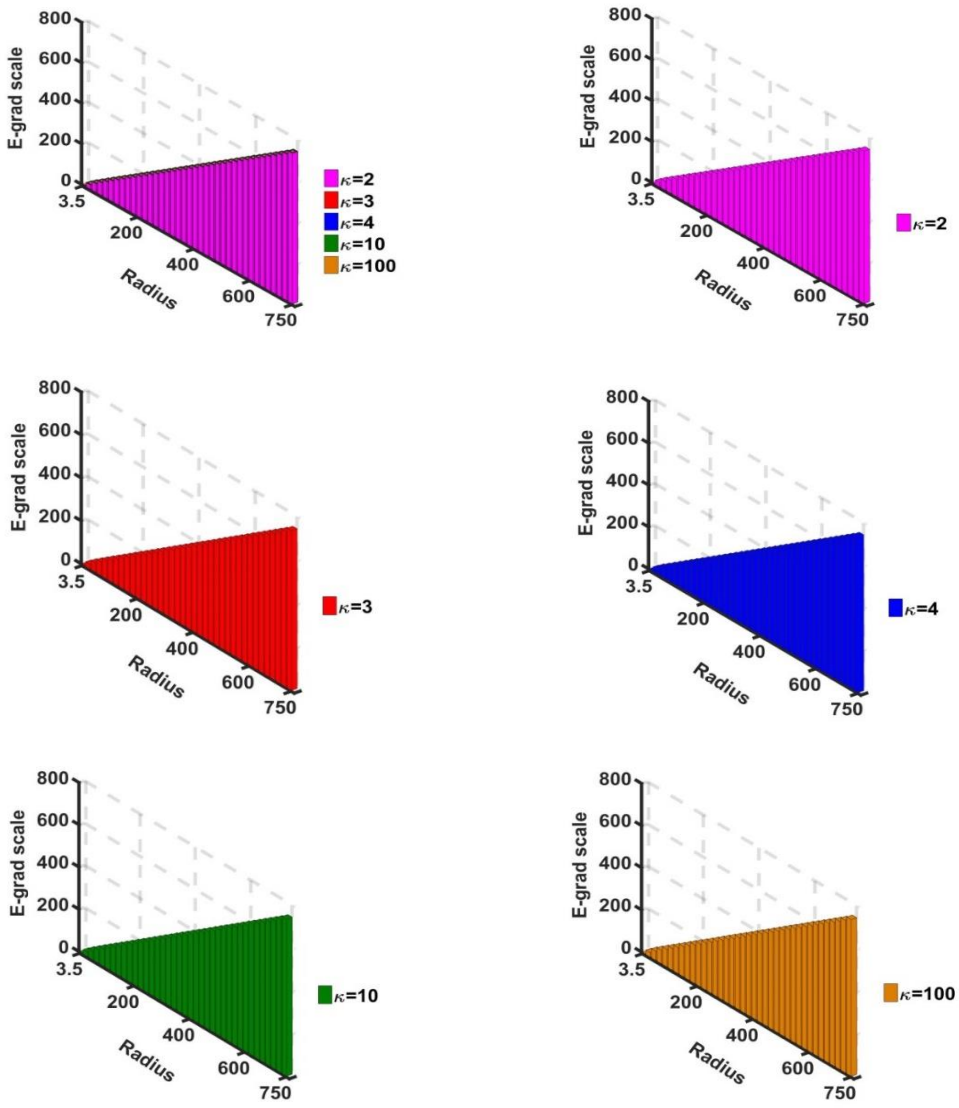

Figure 3.11: *Variation of the normalized SWP electric field inhomogeneity (E-grad) scale length with the Jeans-normalized heliocentric radial distance for fixed $T_e/T_i=1$ and different κ-values as shown.*

We present the SWP Mach number inhomogeneity scale length (= $M(\partial M/\partial\xi)^{-1}$) with the Jeans-normalized heliocentric radial distance for different κ-values in figure 3.12. It is seen that this scale length is independent of the electron non-thermality and maintains a steady growth as the observer moves outward from the SIP. So, the Mach number becomes increasingly more homogeneous in nature towards the far-SIP region.

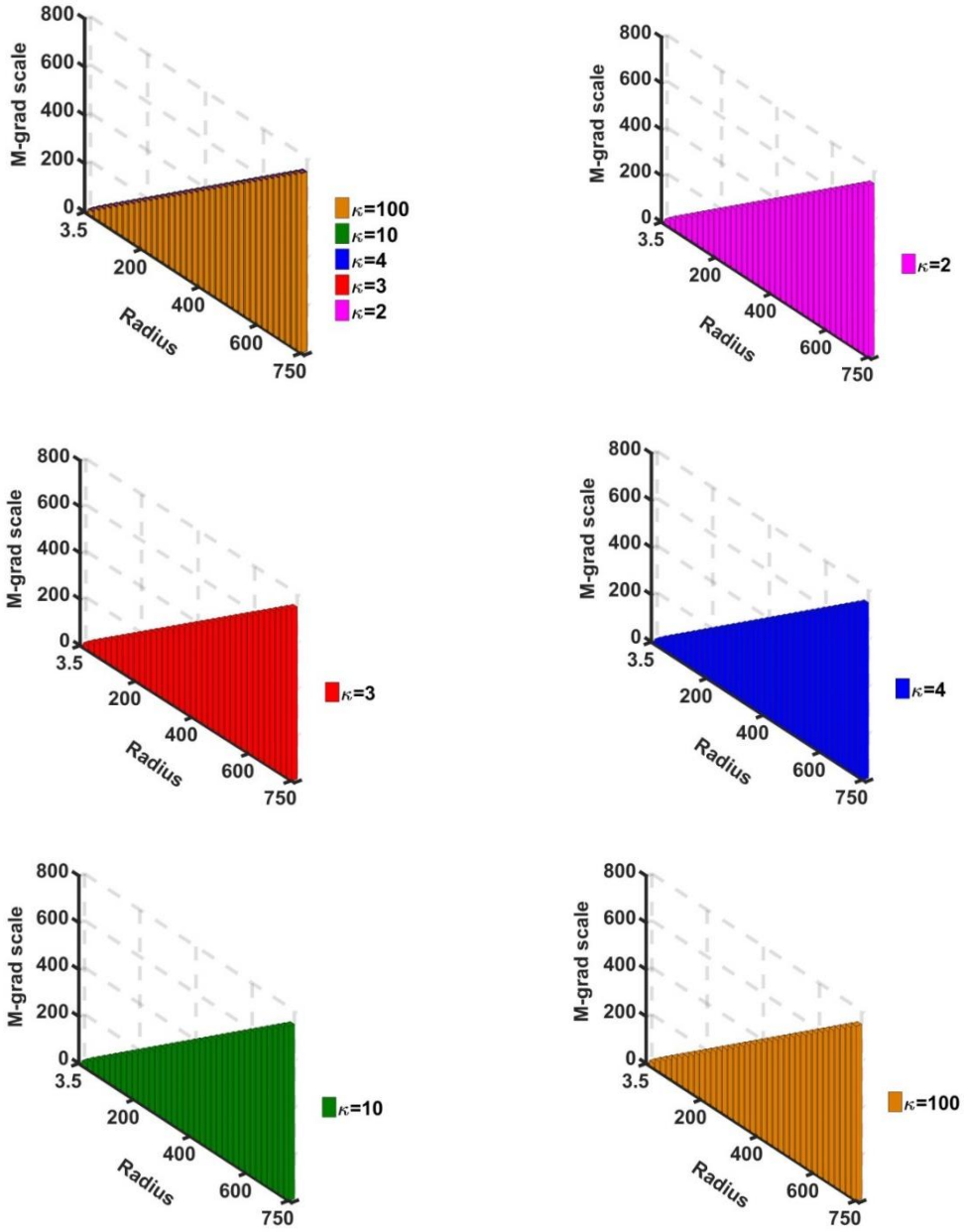

Figure 3.12: *Variation of the normalized SWP Mach number inhomogeneity (M-grad) scale length with the Jeans-normalized heliocentric radial distance for fixed $T_e/T_i=1$ and different κ-values as shown.*

As in figure 3.13, we portray the SWP current density inhomogeneity scale length (= $J(\partial J/\partial\xi)^{-1}$) with the Jeans-normalized heliocentric radial distance for different κ-values. It is seen that this scale length decreases in magnitude in the SWP with increase in electron thermality except in the near-SIP zone. So, the current density becomes homogeneous with decrease in the electron thermality for the most part of the SWP.

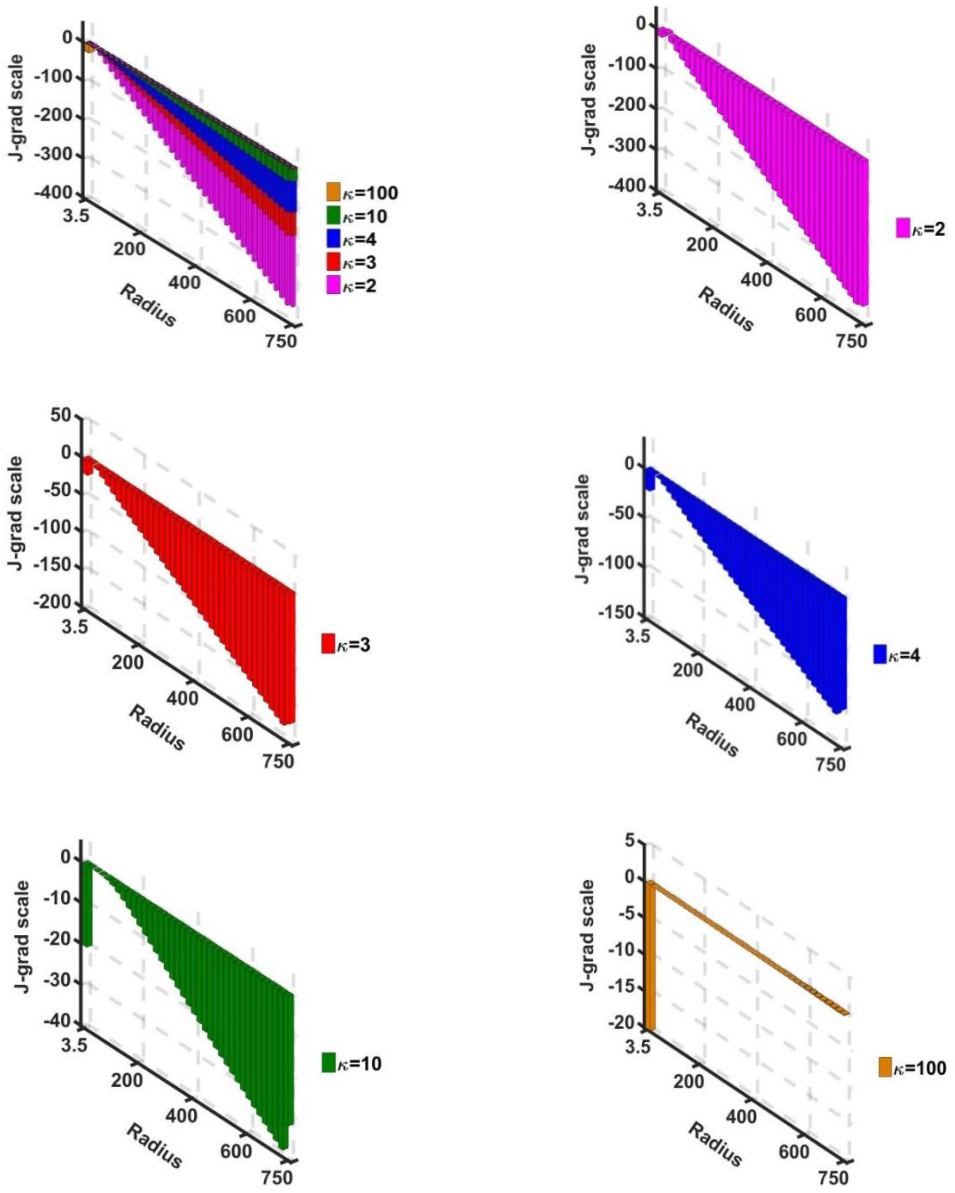

Figure 3.13: *Variation of the normalized SWP electric current density inhomogeneity (J-grad) scale length with the Jeans-normalized heliocentric radial distance for fixed $T_e/T_i=1$ and different κ-values as shown.*

In figure 3.14, we plot the same profile as in figure 3.13, but for different T_e/T_i-values with a particular electron non-thermality. It is found that the magnitude of this inhomogeneity scale length is independent of this ratio in a fixed κ-value. So, the gravito-thermal coupling between the constituents does not affect this scale length.

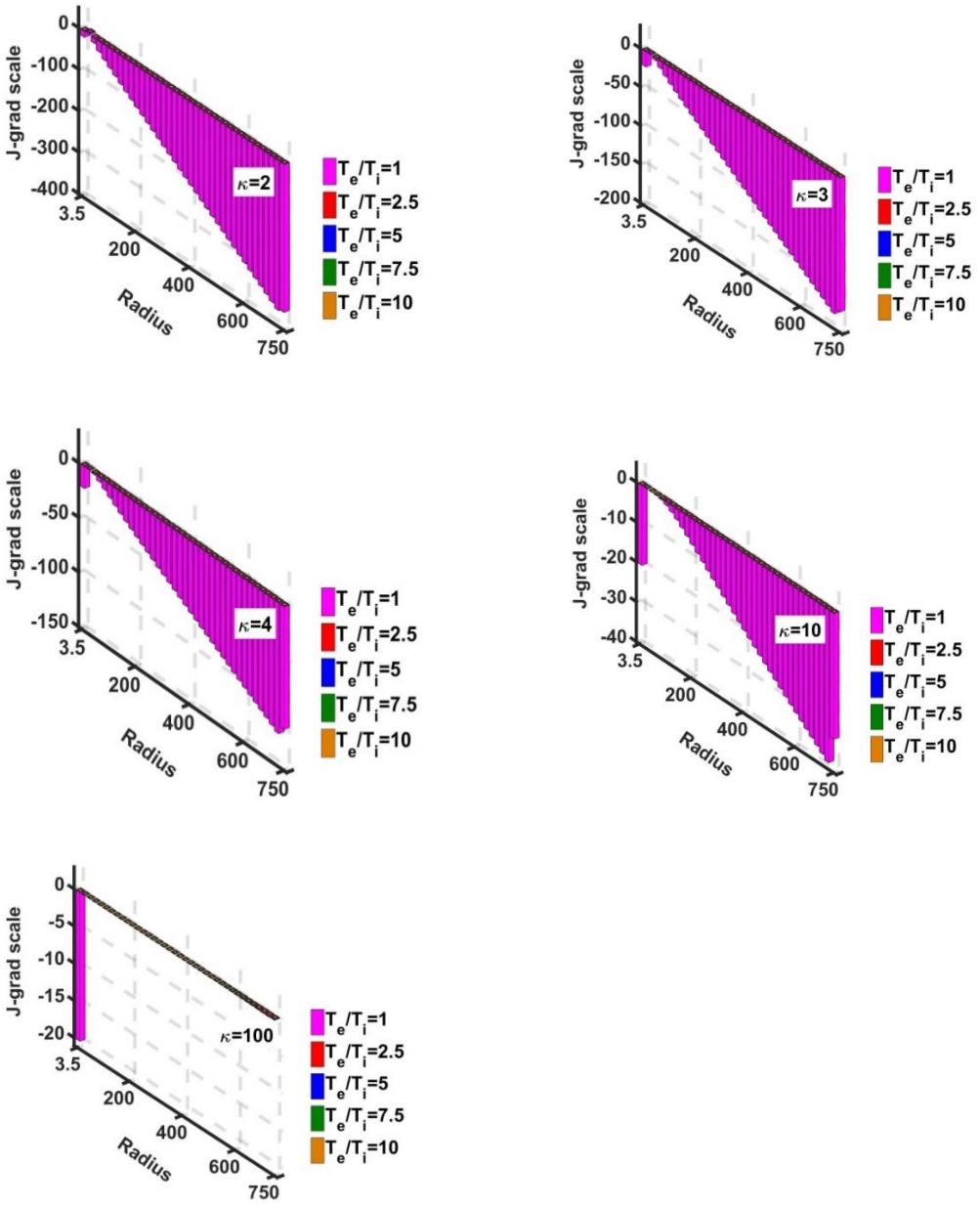

Figure 3.14: *Variation of the normalized SWP electric current density inhomogeneity (J-grad) scale length with the Jeans-normalized heliocentric radial distance for fixed κ and different T_e/T_i–values as shown.*

3.4 CONCLUSIONS

In the presented study, the refined GES-model based solar plasma system by sensibly incorporating the non-thermal electronic thermo-statistics (indicated by the κ-value), magneto-activity, and plasma fluidic turbulence is revisited. Numerical analysis of the model governing equations is performed for both the SIP and the SWP media to plot the inhomogeneity scale lengths of the key solar plasma properties, for studying their spatial

non-uniformity behaviours. It includes the gravito-electrostatic field strengths, electric potential, Mach number, and electric current density. The analysis is performed for various electronic non-thermality levels and relative temperatures of the plasma constituents. It is seen that the SIP self-gravity (figure 3.3) and electric current density (figures 3.7-3.8) show abrupt spatial uniformity transitions. On the other hand, the SWP gravity (figure 3.9), electric potentials (figure 3.4 and figure 3.10), and electric fields (figure 3.5 and figure 3.11) in both the SIP and SWP, Mach number in both the SIP and SWP (figure 3.6 and figure 3.12), and SWP electric current (figures 3.13-3.14) depict gradual spatial uniformity features of a unique type in the entire solar plasma system.

REFERENCES

[1] Pierrard, V. and Lazar, M. Kappa distributions : theory and applications in space plasmas. *Solar Physics*, 267, 153:153-174, 2010.

[2] Livadiotis, G. and McComas, D. J. Understanding kappa distributions: a toolbox for space science and astrophysics. *Space Science Reviews*, 175:183–214, 2013.

[3] Yoon, P. H., Sarfraz, M., Ali, Z., Salem, C. S., and Seough, J. Proton cyclotron and mirror instabilities in marginally stable solar wind plasma. *Monthly Notices of the Royal Astronomical Society*, 509(4):4736-4744, 2022.

[4] Chen, F. F. *Introduction to Plasma Physics and Controlled Fusion*. Springer, New York, 1984.

[5] Vazquez-Semadeni, E., Canto, J., and Lizano, S. Does turbulent pressure behave as a logatrope? *Astrophysical Journal*, 492:596-602, 1998.

[6] Dwivedi, C. B., Karmakar, P. K., and Tripathy, S. C. A gravito-electrostatic sheath model for surface origin of subsonic solar wind plasma. *Astrophysical Journal*, 663:1340-1353, 2007.

[7] Sarma, P. and Karmakar, P. K. Solar plasma characterization in Kappa (κ)-modified polytropic turbomagnetic GES-model perspective. *Monthly Notices of the Royal Astronomical Society*, 519(2):2879-2916, 2023.